Available online at www.sciencedirect.com
ScienceDirect
Journal of the European Ceramic Society 30 (2010) 2165–2171
www.elsevier.com/locate/jeurceramsoc

Stress measurements in ZrB_2–SiC composites using Raman spectroscopy and neutron diffraction

Jeremy Watts [a,*], Greg Hilmas [a], William G. Fahrenholtz [a], Don Brown [b], Bjorn Clausen [b]

[a] *Missouri University of Science and Technology, USA*
[b] *Lujan Center, Los Alamos National Laboratory, USA*

Available online 17 March 2010

Abstract

Raman spectroscopy and neutron diffraction were used to study the stresses generated in zirconium diboride–silicon carbide (ZrB_2–SiC) ceramics. Dense, hot pressed samples were prepared from ZrB_2 containing 30 vol% α-SiC particles. Raman patterns were acquired from the dispersed SiC particulate phase within the composite and stress values were calculated to be 810 MPa. Neutron diffraction patterns were acquired for the ZrB_2–SiC composite, as well as pure ZrB_2 and SiC powders during cooling from ~1800 °C to room temperature. A residual stress of 775 MPa was calculated as a function of temperature by comparing the lattice parameter values for ZrB_2 and SiC within the composite to those of the individual powders. The temperature at which stresses began to accumulate on cooling was found to be ~1400 °C based on observing the deviation in lattice parameters between pure powder samples and those of the composite.

Keywords: Composites; Residual stress; Thermal expansion; Borides; SiC

1. Introduction

Zirconium diboride (ZrB_2) belongs to a class of materials known as ultra-high temperature ceramics, which exhibit melting temperatures in excess of 3000 °C.[1,2] The refractory diborides are generally resistant to chemical attack; this in addition to its high melting point has led to interest in ZrB_2 as a material for molten metal crucibles.[3] Along with high melting temperature and chemical resistivity, zirconium diboride composites, specifically those produced using silicon carbide (SiC) additives, display a wide variety of desirable properties. ZrB_2–SiC composites have been shown to have strengths in excess of 1000 MPa[4–6] and hardness values of 22 GPa and higher.[4,5,7] Zirconium diboride's unusual combination of properties have resulted in interest for uses in refractory linings,[8–10] microelectronics,[11] electrodes,[12–14] cutting tools,[3,15] as well as for use in future aerospace vehicles.[16–18]

The addition of SiC to ZrB_2 has been shown to improve its strength,[4–6,19–21] oxidation resistance,[21–23] and fracture toughness[4,19]; all important factors for potential use in aerospace applications. These effects are believed to be due in part to the stresses generated in and around SiC particles as these materials are cooled from the processing temperature. The room temperature coefficient of thermal expansion (CTE) of ZrB_2 is approximately 5.2 ppm/K[2,24] while the CTE of the 6H polytype of α-SiC is approximately 3.3 ppm/K.[24] As a result, as these materials are cooled from their final densification temperature (typically >1800 °C), compressive stresses are generated in the SiC particles and corresponding tensile stresses are generated in the ZrB_2 matrix as it tries to shrink at a faster rate than the SiC. Raman spectroscopy is one method for measuring stresses in solids. Unfortunately ZrB_2 is not Raman active; however, SiC is. The Raman patterns obtained from Raman active materials provide information similar to other spectroscopic techniques in that the pattern is unique to that specific material. The locations of the peaks present in a Raman pattern are also sensitive to stress.[25–29] While no general relationship equating peak shift to stress has been established, calibration curves have been experimentally obtained for a variety of materials making it possible to correlate peak shift to the stress that material is experiencing.[28,30,31] One limitation of Raman spectroscopy is that it is surface sensitive for opaque materials such as SiC. Neutron diffraction, on the other hand, is capable of providing lattice spacing data from the bulk of a sample, not just at the surface. As a result, neutron

* Corresponding author.
E-mail address: jwatts@mst.edu (J. Watts).

0955-2219/$ – see front matter © 2010 Elsevier Ltd. All rights reserved.
doi:10.1016/j.jeurceramsoc.2010.02.014

diffraction can be used to measure the internal stresses within a material by comparing the measured peak positions to the known peak positions from stress free materials.

The goal of the current study was to measure the residual stresses that develop in hot pressed ZrB_2–SiC composites during cooling from the final densification temperature. This was accomplished using both Raman spectroscopy and neutron diffraction. Raman data was collected on individual SiC particles (~2 μm in size) within the composite. Special samples had to be prepared in order to collect neutron diffraction data. While naturally occurring boron consists of 80% ^{11}B and 20% ^{10}B the high neutron absorption cross section of ^{10}B (3835 b)[32] makes neutron diffraction impractical. The absorption cross section of ^{11}B however is only 0.0055 b.[32] In light of this, samples were produced via reactive hot pressing using ZrH_2 and ^{11}B powder precursors to produce ZrB_2 composites suitable for neutron diffraction studies. Three samples were then prepared for neutron diffraction: pure $Zr^{11}B_2$, pure SiC, and a composite consisting of 70 vol% $Zr^{11}B_2$ with 30 vol% SiC. Neutron diffraction patterns were gathered on all three samples at temperature intervals ranging from room temperature to 1750 °C to determine the total magnitude of stress present as well as to determine the temperature at which stresses begin to accumulate during cooling.

2. Experimental procedure

2.1. Materials and processing

Two powder preparation methods were used in this study. The samples prepared for Raman characterization were produced from ZrB_2 powder (H.C. Starck, Grade B, Goslar, Germany) and SiC powder (H.C. Starck, Grade UF-25). The UF-25 SiC is an alpha-SiC consisting primarily of the 6H polytype. A mixture of 70 vol% ZrB_2 and 30 vol% SiC powder was then attrition milled using WC milling media in a Teflon lined vessel and acetone for a duration of 2 h. Following attrition milling the acetone was removed from the milled slurry using rotary evaporation. The dried powder was then passed through a 60-mesh sieve in order to facilitate uniform die filling later in the process. The samples for neutron diffraction were prepared reactively using ZrH_2 (Alfa Aesar, Grade Z-1038, Ward Hill, MA, USA), boron (Eagle Picher Boron Products, Isotopic enriched boron 11 metal, Quapaw, OK, USA) and the same SiC as above. These powders were ball milled in a polyethylene jar for 12 h using acetone and WC milling media in place of attrition milling for 2 h as was done for the other samples in an effort to affect the same particle size reduction while minimizing WC contamination. The solvent was then removed using rotary evaporation and the dried powders were passed through a 60-mesh sieve.

Both compositions were hot pressed in 44 mm diameter circular graphite dies. The hot press dies were lined with graphoil and the ends of the rams, which would be in contact with the powder, were coated with boron nitride spray (Cerac, SP-108, Milwaukee, WI, USA). After the powder was loaded into the die, it was cold pressed to ~6 MPa. All densification in this study was performed using a resistively heated graphite element hot press (Thermal Technology Inc., Model HP20-3060-20, Santa Rosa, CA, USA). Below 1650 °C, samples were heated under mild vacuum (~20 Pa). The sample being prepared reactively was heated at ~5 °C/min up to 700 °C for the ZrH_2 and ^{11}B to react to form ZrB_2. The non-reactive sample was heated directly to the first hold temperature (1450 °C) at a rate of ~75 °C/min. For both compositions, the powder compact was then heated successively to hold temperatures of 1450 °C and 1650 °C to facilitate the removal of oxide species from the surfaces of the powders. After the 1650 °C hold the furnace atmosphere was changed from vacuum to argon, a hydraulic ram pressure of 32 MPa was applied, and the temperature was raised at ~60 °C/min to 1900 °C. The movement of the hot press rams was monitored and used to determine when densification had ceased. Once ram travel had ceased, the furnace power was turned off and the furnace was allowed to cool (~50 °C/min from 1900 °C to below 600 °C). Load on the sample was maintained until the temperature fell to 1650 °C and was then removed. Powder specimens for neutron diffraction were prepared by reacting ZrH_2 and ^{11}B powders up to 1450 °C and crushing the resulting material to −325 mesh for the $Zr^{11}B_2$ while the SiC was used as received.

After hot pressing, billets were removed from the die and surface ground in order to make the surfaces flat and parallel as well as remove any boron nitride adhering to the specimen surfaces. Each billet was then cut into bars ~2.5 mm in width. Finally the bars were ground to obtain final cross sectional dimensions of 1.5 mm × 2 mm with a 400-grit finish. All cutting and grinding was done with diamond abrasive wheels on an automated surface grinder (Chevalier, FSG-3A818, Santa Fe Springs, CA). Specimens prepared for Raman measurements and microscopy were polished to a 0.25 μm diamond finish.

2.2. Characterization

Archimedes' density measurements were made for each billet. After the dry weight was recorded, samples were saturated by submersion in distilled water and placing them under vacuum for 12 h. The saturated and suspended weights were then measured to calculate a final density. Microstructural analysis was performed using a Hitachi S570 scanning electron microscope (Tokyo, Japan). Particle size was determined using ImageJ software by analyzing ~500 grains. X-ray diffraction analysis was performed using a Philips X-Pert Pro diffractometer (Westborough, MA, USA).

Stress values were obtained using both Raman spectroscopy and neutron diffraction. Raman measurements were made using a Horiba LabRAM ARAMIS spectrometer (Edison, NJ, USA) using a 633 nm HeNe laser and a 1 μm spot size. Before the dataset was obtained the instrument was calibrated using a silicon standard, and data was collected up to 1000 wave numbers. Raman patterns were gathered only from the SiC within the ZrB_2–SiC composite material due to ZrB_2 being Raman inactive. Data was gathered from 25 separate SiC particulates within the microstructure. Neutron diffraction was performed using the time of flight (TOF) method in the Lujon Center at Los Alamos National Lab using the Spectrometer for Materials Research at Temperature and Stress (SMARTS). Specimens for neutron

Table 1
Final density and SiC particle size of the reactively and traditionally produced specimens.

Composition	Theoretical density (g/cm^3)	Archimedes density (g/cm^3)	Average SiC particle size (μm)
30 vol% SiC 70 vol% ZrB_2	5.24	5.32	3.3
30 vol% SiC 70 vol% $Zr^{11}B_2$	5.25	5.38	2.0

diffraction consisted of 5 bars (1.5 mm × 2 mm × 15 mm) contained in an alumina crucible; the crucible was placed inside a tungsten element furnace situated in the path of the neutron beam. The specimens were heated to a maximum temperature of 1750 °C under vacuum (1×10^{-4} Torr) at a rate of 20 °C/min. Neutron diffraction patterns were collected at various temperatures upon both heating and cooling. Temperature was allowed to equilibrate for 15 min prior to each measurement. Data was then gathered for approximately 1 h at each temperature. Diffraction data was collected for a composite material consisting of 70 vol% $Zr^{11}B_2$ and 30 vol% SiC as well as for the individual $Zr^{11}B_2$ and SiC powders.

3. Results and discussion

Final densities and SiC particle sizes were measured for both the ZrB_2–SiC and $Zr^{11}B_2$–SiC composite materials (Table 1) to ensure that microstructures and densities were similar. Both materials were hot pressed to full density as measured by Archimedes' technique. As can be seen in Table 1 both materials actually reached a slightly higher density than predicted based on the nominal composition of 70 vol% ZrB_2 and 30 vol% SiC. This was due to the incorporation of small amounts of WC milling media used; approximately 2 wt% WC was in the ZrB_2–SiC composite and 4 wt% was in the $Zr^{11}B_2$–SiC composite as determined by the mass loss of the milling media. The microstructures of both materials consisted of a ZrB_2 matrix containing a fine, well-dispersed SiC second phase (Fig. 1). The SiC particulate size in the reaction processed specimen (~2 μm) was slightly smaller than for the conventionally hot pressed specimen (~3 μm). This is consistent with previously reported results.[7] Given the similarity in microstructures there should not be a significant difference in stress evolution during processing between the two materials.

A Raman pattern (Fig. 2) obtained from the SiC particles in the hot pressed ZrB_2–30 vol% SiC specimen shows measurable peak shifts in the wave number for both the transverse optic (TO) and linear optic (LO) peaks. The TO and LO peaks have been shifted by 2.5 cm^{-1} and 3.9 cm^{-1}, respectively, to higher wave numbers. Fig. 2 illustrates how the peaks in the Raman pattern of stressed SiC shift away from the standard, unstressed locations. This phenomenon has been studied for a number of materials and can be used to calculate the internal stress of the material being analyzed.[26,31,33]

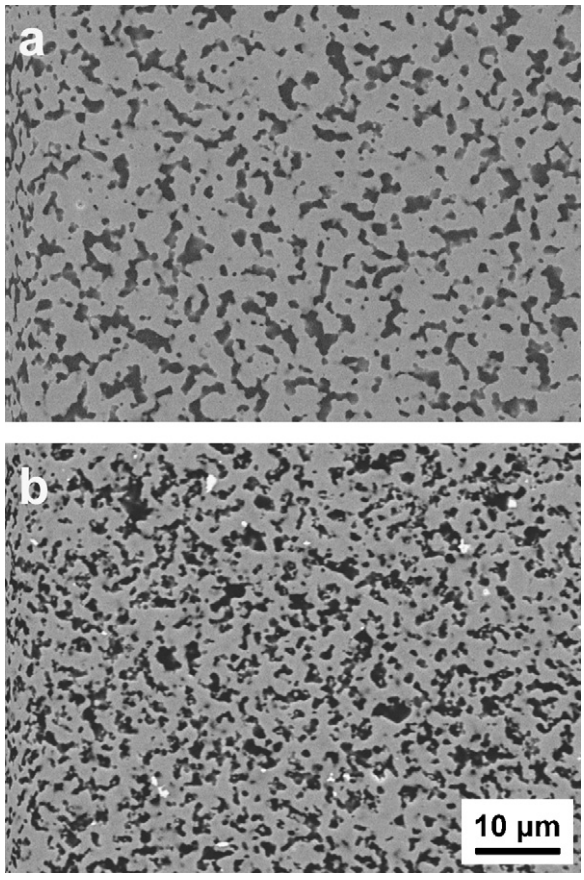

Fig. 1. Microstructural comparison of conventionally hot pressed ZrB_2–SiC (a) with reaction hot pressed $Zr^{11}B_2$–SiC (b).

Liu and Vohra[26] analyzed Raman peak shifting of 6H SiC as a function of applied hydrostatic pressure from ambient up to 90 GPa compressive stress. Further, they were able to develop an equation (Eq. (1)) to correlate the magnitude of peak shift to the internal stress in 6H SiC.[26]

$$\omega_{TO}(cm^{-1}) = 789.2 + 3.11P - 0.009P^2 \quad (1)$$

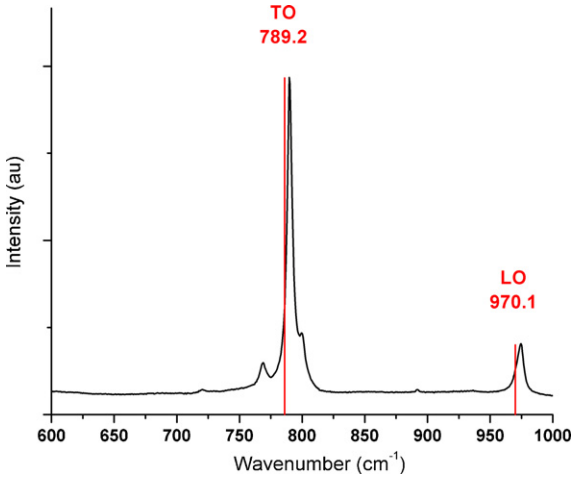

Fig. 2. Raman pattern for 6H SiC from a hot pressed ZrB_2–SiC composite with unstressed peak positions identified with lines.[26]

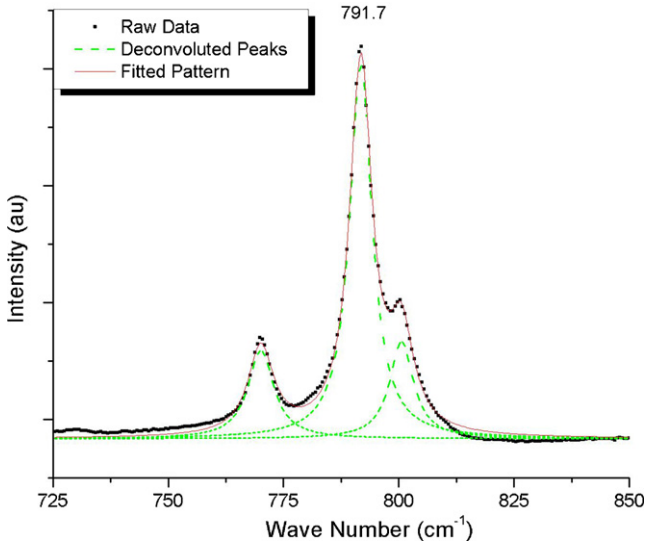

Fig. 3. Representative raw Raman spectrum from an individual SiC particle as well as deconvoluted peak fits to determine true peak position.

In this equation ω_{TO} refers to the peak position of the transverse optical (TO) peak, and P is the internal stress in GPa. Using the unstressed position of the TO peak (789.2 cm^{-1}),[26] and combining that term with the ω_{TO} term and solving for P, a second equation which allows for the calculation of internal stress by inputting the amount of peak shift (ΔTO) is obtained (Eq. (2)).

$$P = \frac{3.11 - \sqrt{9.6721 - 0.036(\Delta TO)}}{0.018} \quad (2)$$

A representative Raman pattern (Fig. 3) acquired from an individual SiC particle in the conventionally hot pressed ZrB_2–30 vol% SiC material shows a TO peak shift of 2.5 cm^{-1}. The TO peak was focused on for this study due to the strength of the peak and the ability to obtain accurate peak fits. When two or more peaks overlap one another, the resultant peak positions are affected due to the additive effect of the multiple peaks. Therefore, it is necessary to deconvolute the peaks to obtain the true peak positions. Fig. 3 is a plot of raw Raman data representative of the dataset along with deconvoluted peak fits to determine the true center of the TO peak.

By inputting the TO peak shift (2.5 cm^{-1}) for ΔTO in Eq. (2), the internal stress in a representative SiC particle was calculated to be approximately 810 MPa (compressive). Using that stress value (σ), along with the elastic moduli (E) and Poisson's ratios (υ) of SiC and ZrB_2, the difference in thermal expansion coefficient ($\Delta\alpha$) between SiC and ZrB_2, and the volume fraction of particulate phase (V_p), it is possible to calculate the temperature at which stresses began to accumulate upon cooling (Eq. (3)). In this equation the subscripts p and m designate particle and matrix respectively.[34]

$$\Delta T = \frac{\sigma(0.5(1+\upsilon_m)+(1-2\upsilon_m)V_p/E_m(1-V_p)+1-2\upsilon_p/E_p)}{\Delta\alpha} \quad (3)$$

While the CTE of both SiC and ZrB_2 change as a function of temperature, the difference in CTE is ~2 ppm/K over the entire processing temperature range. By inputting that value for $\Delta\alpha$, 415 GPa[35] for E_p, 489 GPa[2] for E_m, 0.14 and 0.16 for υ_m[36] and υ_p[35] respectively, and the measured compressive stress of 810 MPa for σ, ΔT is found to be 1595 °C. Taking into account that the stress was measured at room temperature, the measurement suggests that stresses started to accumulate at approximately 1620 °C during cooling. It is also important to note here that Raman spectroscopy is a surface sensitive characterization technique. Therefore, the stresses measured on a free surface of the sample could be different than those that exist in the bulk of the material.

Neutron diffraction, on the other hand, allows in-situ measurement of the internal strains in the bulk of the material as the specimen is heated to near the processing temperature and then cooled. Fig. 4 illustrates the lattice parameters for the (0 0 6) SiC plane between a powder specimen (i.e., no residual stress due to CTE mismatch with a matrix phase) and SiC in the $Zr^{11}B_2$–30 vol% SiC specimen. Diffraction data was collected as the specimen was cooled from 1750 °C to room temperature. The CTE was measured for the SiC powder based on the shift in lattice parameter as a function of temperature. Fitting the data with a 3rd order polynomial shows good agreement with data in the literature[24,35] and results in a room temperature CTE of 3.7 ppm/°C.

At temperatures of 1500 °C and higher, the lattice parameters of the powder and the composite overlapped one another as is expected when both materials are stress free. However, at some temperature between 1500 °C and 1200 °C the lattice parameters of the two materials begin to deviate. The major reason for the two lattice parameters to differ from each other as a function of temperature was the stress generated in the composite specimen during cooling due to its CTE mismatch with the ZrB_2 matrix. Knowing that at 1200 °C and below the lattice parameters differed between powder and composite, the

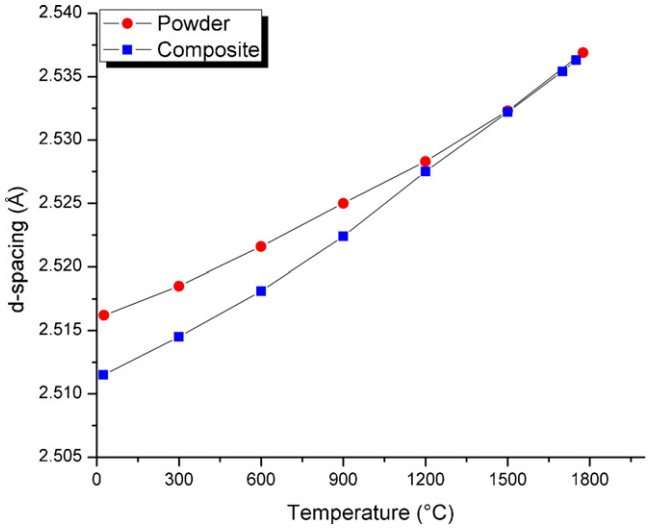

Fig. 4. The (0 0 6) lattice parameter of both SiC powder and SiC within the $Zr^{11}B_2$–SiC composite as a function of temperature during cooling from 1775 °C.

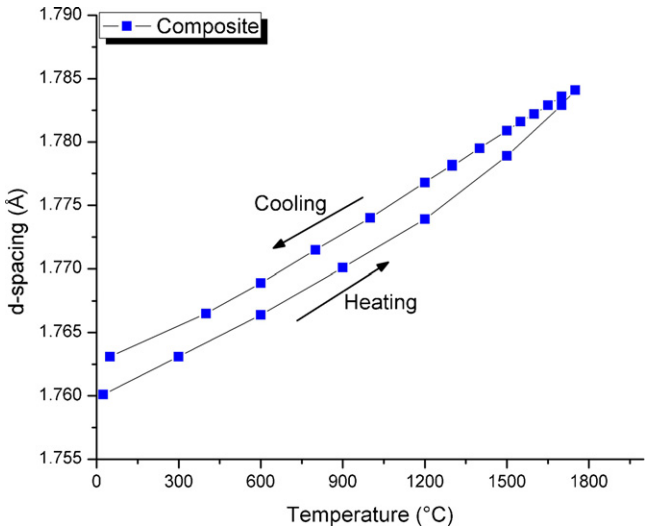

Fig. 5. The (0 0 2) lattice parameter for $Zr^{11}B_2$ in the composite deviating from itself between heating and cooling.

composite lattice parameter data below 1200 °C was fit with a second order polynomial and extrapolated to higher temperature. This resulted in the extrapolated fit intercepting the powder lattice parameter at ~1400 °C. The room temperature lattice parameter difference between the powder and composite specimens was measured to be 0.0047 Å, which equates to a strain of 0.187%. By relating the strain to stress using the elastic modulus, the stress within the SiC was found to be ~775 MPa (compressive).

In order to determine if the ΔT values calculated from the Raman stress measurements were reasonable, a similar calculation was performed using the stress of 775 MPa calculated from neutron diffraction and the ΔT range known from the lattice parameter measurements. Inputting 775 MPa into Eq. (3) yields a temperature where stresses begin to accumulate of ~1550 °C, which is higher than the 1400 °C predicted by neutron diffraction. However, further investigation into the neutron diffraction data revealed that more than just a CTE mismatch between ZrB_2 and SiC affected the lattice parameter shifts within the composite.

The lattice parameters for ZrB_2 in the composite should be shifted as compared to those of the standard powder due to internal stresses. However, they should be self-consistent between heating and cooling cycles. The (0 0 2) lattice parameter measured for the ZrB_2 within the composite (Fig. 5), differed at any given temperature during heating and cooling. The lattice parameter became larger as temperature increased, as expected due to thermal expansion. However during cooling, the lattice parameter decreased, but remained larger than it was on heating over the entire temperature range. Fig. 5 illustrates how the (0 0 2) lattice parameter of ZrB_2 within the composite changed during heating and cooling. The deviation between heating and cooling likely indicated a compositional change within the composite that was shifting the lattice parameters after prolonged exposure to high temperatures.

Microscopy analysis was used to investigate the compositional changes in the $Zr^{11}B_2$–30 vol% SiC specimen after

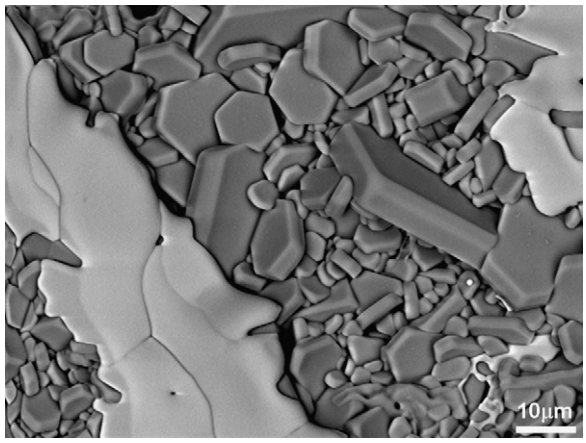

Fig. 6. Backscatter SEM image of the surface of a sample exhibiting a high z-contrast second phase generated during the neutron diffraction experiment.

elevated temperature neutron diffraction. The SEM images revealed the presence of a third phase (Fig. 6) in addition to ZrB_2 and SiC. This third phase presumably evolved during the high temperature portion of the experiment. Energy dispersive spectroscopy (EDS) indicated that the third phase was rich in tungsten and silicon. Fig. 6 is a backscattered SEM image of the surface of the specimen showing the presence of a high z-contrast phase with respect to ZrB_2. X-ray diffraction performed on that same specimen also indicated the presence of the third phase, which exhibited diffraction peaks consistent with WSi_2 (Fig. 7). Fig. 7 illustrates the presence of three peaks consistent with WSi_2 in what is otherwise a typical ZrB_2 diffraction pattern. Neither XRD nor SEM indicated the presence of this phase prior to the neutron diffraction experiment. Based on the introduction of WC into the specimen during milling, it appears that the W went into solid solution during processing, and stayed in solution after the relatively rapid cooling (~100 °C/min) following densification. During the neutron diffraction experiment however, the specimen was held at various temperatures below

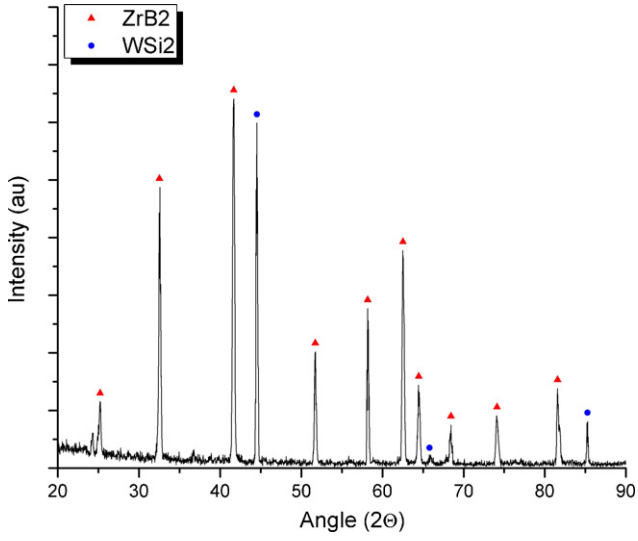

Fig. 7. X-ray diffraction spectrum from the surface of a sample exhibiting a second phase consistent with WSi_2.

the densification temperature for over an hour at each temperature while the neutron diffraction pattern was being collected. It appears that the WC (or just the W) came out of solution and reacted with the SiC to form WSi_2. The exsolution of WC (or W) from ZrB_2 would be expected to increase the lattice parameters as measured via neutron diffraction since W has a smaller covalent radius than Zr.[37]

The stress calculated from Raman spectroscopy peak shifts (810 MPa) was slightly higher than that calculated from neutron diffraction analysis (775 MPa). This is counterintuitive based on the notion that the particles analyzed using Raman were on a free surface, which would presumably reduce stress compared to the bulk by releasing part of the constraint on the particle. While neutron diffraction has been extensively used to measure the internal stresses of composite materials,[38–41] it has also been shown that the measured lattice parameter shifts expected due to CTE mismatch can be altered by changes in chemistry.[42] If the third phase had the same effect on the SiC as on the ZrB_2, that of increasing the lattice parameter, it would mask some of the contraction in lattice parameter due to compressive stress and could result in a lower measured stress. In light of this, further neutron diffraction experiments could benefit from production of samples without any WC impurity to confirm the SiC lattice parameter data and collect complementary data for lattice parameter changes and residual stresses in ZrB_2.

4. Conclusions

Raman spectroscopy and neutron diffraction were used to determine the stresses generated in SiC particles within ZrB_2–SiC composites during processing. Peak shifts measured by Raman spectroscopy were consistent with a compressive stress of ~810 MPa at room temperature, which corresponds to a zero stress temperature of ~1620 °C during cooling from the densification temperature. $Zr^{11}B_2$–SiC composites were successfully fabricated using ^{11}B isotope. Lattice parameters for the composite were measured using neutron diffraction from room temperature up to 1750 °C. Lattice parameter changes in the SiC indicated a compressive stress of ~775 MPa and a zero stress temperature of ~1400 °C. The discrepancy between $Zr^{11}B_2$ lattice parameters on heating and cooling, as well as subsequent XRD and SEM analysis, suggest that the WC impurity introduced during milling caused compositional changes and thus altered lattice parameters during the experiment.

Acknowledgements

This work has benefited from the use of the Lujan Neutron Scattering Center at LANSCE, which is funded by the Office of Basic Energy Sciences (DOE).

Los Alamos National Laboratory is operated by Los Alamos National Security LLC under DOE Contract DE AC52 06NA25396. Research at Missouri S&T was supported by the High Temperature Aerospace Materials Program (Dr. Joan Fuller, program manager) in the Air Force Office of Scientific Research through grant FA9550-09-1-0168.

References

1. Cutler RA. Engineering properties of borides. In: Schneider Jr SJ, editor. *Ceramics and glasses, engineered materials handbook*, vol. 4. Materials Park, OH: ASM International; 1991. p. 787–803.
2. Fahrenholtz WG, Hilmas GE, Talmy IG, Zaykoski JA. Refractory diborides of zirconium and hafnium. *Journal of the American Ceramic Society* 2007;**90**(5):1347–64.
3. Mishra SK, Das S, Das SK, Ramachandrarao P. Sintering studies on ultrafine ZrB_2 powder produced by a self-propagating high-temperature synthesis process. *Journal of Materials Research* 2000;**15**(11):2499– 504.
4. Chamberlain AL, Fahrenholtz WG, Hilmas GE, Ellerby DT. High-strength zirconium diboride-based ceramics. *Journal of the American Ceramic Society* 2004;**87**(6):1170–2.
5. Henderson S, Fahrenholtz WG, Hilmas GE, Marschall J. High-velocity impact resistance of ZrB2–SiC. In: A. W. E. L.-C., *Mechanical properties and performance of engineering ceramics ii: ceramic engineering and science proceedings*, *issue* 2, vol. 27. 2008. p. 3–9.
6. Rezaie A, Fahrenholtz WG, Hilmas GE. Effect of hot pressing time and temperature on the microstructure and mechanical properties of ZrB_2–SiC. *Journal of Materials Science* 2007;**42**(8):2735–44.
7. Chamberlain AL, Fahrenholtz WG, Hilmas GE. Low-temperature densification of zirconium diboride ceramics by reactive hot pressing. *Journal of the American Ceramic Society* 2006;**89**(12):3638–45.
8. Motojima S, Funahashi K, Kurosawa K. ZrB_2 coated on copper plate by chemical vapour deposition, and its corrosion and oxidation stabilities. *Thin Solid Films* 1990;**189**(1):73–9.
9. Kida O. Monolithic refractory material and waste melting furnace using the same. J. Patent, JP2000335969; 2000.
10. Kaji N, Shikano H, Tanaka I. Development of ZrB_2–graphite protective sleeve for submerged nozzle. *Taikabutsu Overseas* 1992;**14**(2):39–43.
11. Sung J, Goedde DM, Girolami GS, Abelson JR. Remote-plasma chemical vapor deposition of conformal ZrB_2 films at low temperature: a promising diffusion barrier for ultralarge scale integrated electronics. *Journal of Applied Physics* 2002;**91**(6):3904–11.
12. Stucker B, Bradley W, Eubank PT, Norasetthekul S, Bozkurt B. Zirconium diboride/copper EDM electrodes from selective laser sintering. *Solid Freeform Fabrication Proceedings* 1997;**1**:257–66.
13. Jin ZJ, Zhang M, Guo DM, Kang RK. Electroforming of copper/ZrB_2 composite coating and its performance as electro-discharge machining electrodes. *Key Engineering Materials* 2005;**291–292**:537–42.
14. Stucker B, Malhorta M, Qu Z. Recent developments in the selective laser sintering of Zykron EDM electrodes. *Proceedings of the laser materials processing conference* 1999;**2**:158–61.
15. Murata Y. Cutting tool tips and ceramics containing hafnium nitride and zirconium diboride. U.S. Patent, 3487594; 1970.
16. Opeka MM, Talmy IG, Zaykoski JA. Oxidation-based materials selection for 2000 °C + hypersonic aerosurfaces: theoretical considerations and historical experience. *Journal of Materials Science* 2004;**39**(19):5887–904.
17. Van Wie DM, Drewry DG, King DE, Hudson CM. The hypersonic environment: required operating conditions and design challenges. *Journal of Materials Science* 2004;**39**(19):5915–24.
18. Jackson TA, Eklund DR, Fink AJ. High speed propulsion: performance advantage of advanced materials. *Journal of Materials Science* 2004;**39**(19):5905–13.
19. Wang H, Wang C-A, Yao X, Fang D. Processing and mechanical properties of zirconium diboride-based ceramics prepared by spark plasma sintering. *Journal of the American Ceramic Society* 2007;**90**(7):1992–7.
20. Monteverde F, Guicciardi S, Bellosi A. Advances in microstructure and mechanical properties of zirconium diboride based ceramics. *Materials Science and Engineering A* 2003;**346**(1–2):310–9.
21. Monteverde F. Beneficial effects of an ultra-fine α-SiC incorporation on the sinterability and mechanical properties of ZrB_2. *Applied Physics A: Materials Science & Processing* 2006;**82**(2):329–37.
22. Peng F, Speyer RF. Oxidation resistance of fully dense ZrB_2 with SiC, TaB_2, and $TaSi_2$ additives. *Journal of the American Ceramic Society* 2008;**91**(5):1489–94.

23. Inna G, Talmy JA, Zaykoski MM, Opeka. High-temperature chemistry and oxidation of ZrB_2 ceramics containing SiC, Si_3N_4, Ta_5Si_3, and $TaSi_2$. *Journal of the American Ceramic Society* 2008;**91**(7):2250–7.
24. Touloukian Y, Ho C, Dewitt D. *Thermal expansion: nonmetallic solids*. New York: IFI/Plenum; 1970.
25. Salvador G, Sherman WF. Pressure dependence of the Raman phonon spectrum in 6H-silicon carbide. *Journal of Molecular Structure* 1991;**247**:373–84.
26. Liu J, Vohra YK. Raman modes of 6H polytype of silicon carbide to ultra-high pressures: a comparison with silicon and diamond. *Physical Review Letters* 1994;**72**(26):4105.
27. Ghosh D, Subhash G, Orlovskaya N. Measurement of scratch-induced residual stress within SiC grains in ZrB_2–SiC composite using micro-Raman spectroscopy. *Acta Materilia* 2008;**56**(18):5345–54.
28. Wu X, Yu J, Ren T, Liu L. Micro-Raman spectroscopy measurement of stress in silicon. *Microelectronics Journal* 2007;**38**(1):87–90.
29. Young RJ, Buschow KHJ, Robert WC, Merton CF, Bernard I, Edward JK, et al. Residual stresses: measurement by Raman shift. In: *Encyclopedia of materials: science and technology.* Oxford: Elsevier; 2001. pp. 8170–8172.
30. Olego D, Cardona M, Vogl P. Pressure dependence of the optical phonons and transverse effective charge in 3C–SiC. *Physical Review B* 1982;**25**(6):3878.
31. Ohtsuka S, Zhu W, Tochino S, Sekiguchi Y, Pezzotti G. In-depth analysis of residual stress in an alumina coating on silicon nitride substrate using confocal raman piezo-spectroscopy. *Acta Materialia* 2007;**55**(4):1129–35.
32. Sears VF. Neutron scattering length and cross sections. *Neutron News* 1992;**3**(3):26–37.
33. DiGregorio JF, Furtak TE, Petrovic JJ. A technique for measuring residual stress in SiC whiskers within an alumina matrix through Raman spectroscopy. *Journal of Applied Physics* 1992;**71**(7):3524–31.
34. Chawla KK. *Composite materials*. New York: Springer-Verlag; 1998. p. 333.
35. Munro RG. Material properties of a sintered alpha-SiC. *Journal of Physical and Chemical Reference Data* 1997;**26**(5):1195–203.
36. Zhang X, Luo X, Han J, Li J, Han W. Electronic structure, elasticity and hardness of diborides of zirconium and hafnium: first principles calculations. *Computational Materials Science* 2008;**44**(2):411–21.
37. Cordero B, Gomez V, Platero-Prats A, Reves M, Echeverria J, Cremades E, et al. Covalent radii revisited. *Dalton Transactions* 2008;(21):2832–8.
38. Bartolomé JF, Bruno G, DeAza AH. Neutron diffraction residual stress analysis of zirconia toughened alumina (ZTA) composites. *Journal of the European Ceramic Society* 2008;**28**(9):1809–14.
39. Ruiz-Hervías J, Bruno G, Gurauskis J, Sánchez-Herencia AJ, Baudín C. Neutron diffraction investigation for possible anisotropy within monolithic Al_2O_3/Y-TZP composites fabricated by stacking together cast tapes. *Scripta Materialia* 2006;**54**(6):1133–7.
40. Todd RI, Bourke MAM, Borsa CE, Brook RJ. Neutron diffraction measurements of residual stresses in alumina/SiC nanocomposites. *Acta Materialia* 1997;**45**(4):1791–800.
41. Wain N, Radaelli PG, Todd RI. In situ neutron diffraction study of residual stress development in MgO/SiC ceramic nanocomposites during thermal cycling. *Acta Materialia* 2007;**55**(13):4535–44.
42. Mari D, Clausen B, Bourke MAM, Buss K. Measurement of residual thermal stress in WC–Co by neutron diffraction. *International Journal of Refractory Metals and Hard Materials* 2009;**27**(2):282–7.